On the Helicity Dynamics of Severe Convective Storms①

Fei Shiqiang (费世强) and Tan Zhemin (谈哲敏)

Laboratory of Meso-scale Severe Weather, Department of Atmospheric Sciences, Nanjing University, Nanjing 210093

P44 A

(Received December 29, 1999; revised August 15, 2000)

ABSTRACT

A well-documented supercell thunderstorm occurred in Del City, Oklahoma, on 20 May 1977 is successfully simulated by a three-dimensional, nonhydrostatic storm-scale numerical model ARPS. With the numerical simulated data of the storm, the structure and evolution of the helicity, superhelicity and their dynamical influences on the development of the storm are investigated. The initial helical structure of environmental flow is favorable to the development of storm. In the developing stage of storm, low helicity is beneficial to the nonlinear energy cascade. However, the high helicity is of help to maintain the energy of convection cell at the mature stage of storm, and lead to a long life cycle of convective cell. Rotating thunderstorm has a tendency of adjusting to the Beltrami flow structure and tends to a higher helicity of flow. The negative superhelicity could lead to an increase of helicity. Superhelicity is negative in the initial developing process of storm however the superhelicity is positive in the mature stage of storm. Therefore, the superhelicity can be used as an indicator of the mature degree of convective storm.

Key words: Convective storm, Helicity, Superhelicity

1. Introduction

Convective storms, such as thunderstorm, squall line, tornadoes and so on, usually develop in the unstable large-scale environment. All of them can be characterized by the strong rotation. Due to the strong rotation and updraft motion, severe weather phenomena such as heavy precipitation and severe wind often occur in the evolution of these systems. Since the spatial scale is small and life cycle is short, the severe storms are very difficult to be recognized and traced during the normal observations. The development and application of the three-dimensional storm-scale numerical model make it possible to understand the detailed dynamic processes of severe storms and to forecast them. Furthermore, in order to understand the dynamical processes and mechanisms deeply, a lot of new physical quantities or dynamic parameters, e.g., helicity and bulk Richardson number have been suggested to measure the development of convective storm.

Helicity (restrictedly helicity density) is defined as the scalar product of velocity and vorticity vector. It describes the motion of fluid in the rotational direction or the rotational characteristics in the motion direction and reflects the twining structure of the vortex tubes. The helicity has the same importance as energy and enstrophy in the three-dimensional flow.

①This research was supported by National Natural Science Foundation of China under the Grant No. 49605064 and 49735180 and by State Key Basic Research Program: Research on the Formation Mechanism and Prediction Theory of Hazardous Weather over China (CHERES, No. G1998040907), and in part by the Isaac Newton Institute for Mathematical Sciences, University of Cambridge.

Helicity is defined as

$$h_v = \vec{v} \cdot \vec{\omega}, \tag{1}$$

where $\vec{v}$ is the three-dimensional wind vector, $\vec{\omega}$ is vorticity vector. The quantity defined in (1) is called the helicity density. In general the helicity is defined as the volume integration of h_v.

Helicity shown in (1) can be expressed as another form

$$h_v = u(\frac{\partial w}{\partial y} - \frac{\partial v}{\partial z}) + v(\frac{\partial u}{\partial z} - \frac{\partial w}{\partial x}) + w(\frac{\partial v}{\partial x} - \frac{\partial u}{\partial y}) = h_x + h_y + h_z \tag{2}$$

where $h_x = u(\frac{\partial w}{\partial y} - \frac{\partial v}{\partial z})$, $h_y = v(\frac{\partial u}{\partial z} - \frac{\partial w}{\partial x})$ and $h_z = w(\frac{\partial v}{\partial x} - \frac{\partial u}{\partial y})$ are the components of helicity produced by the x-, y- and z-direction vorticity, respectively.

The normalized helicity density i.e., relative helicity density is defined as follows:

$$D_{nh} = \frac{\vec{v} \cdot \vec{\omega}}{|\vec{v}||\vec{\omega}|} = \cos\alpha, \tag{3}$$

where α is the angle between the velocity vector and vorticity vector. Obviously, $-1 \leqslant D_{nh} \leqslant 1$. Therefore, D_{nh} measures the coherence of velocity and vorticity field.

When the velocity and vorticity vectors are parallel everywhere, i.e., D_{nh} is maximum, then we have

$$\vec{\omega} = \lambda \vec{v}, \tag{4}$$

where λ is constant and determines the sign of helicity. Similarly, (4) implies that

$$\vec{\omega} \cdot \vec{v} = 0. \tag{5}$$

If the motion satisfies (5), the flow is called the Beltrami flow (Lilly, 1986; Elting, 1985).

In order to investigate the influences of the environmental parameters on the development of severe storm, Davies-Jones et al. (1990) defined the storm-relative helicity (SREH) of low-level environment flow as

$$h_{sre} = \int_0^h [(\vec{v} - \mathbf{c}) \cdot \vec{\omega}_h] dz \tag{6}$$

where $\vec{v}$ is the environmental velocity and $\mathbf{c}$ is the moving speed of storm. Clearly, $\vec{v} - \mathbf{c}$ is the inflow vector of storm. $\vec{\omega}_h$ is the horizontal vorticity vector. h refers to a certain height above the surface and is usually taken as 2 km or 3 km. h_{sre} depends on the horizontal components of the vorticity and the storm inflow that can reflect the potential rotation of the environment field.

Moffat (1969) showed that the helicity is conservative in the inviscous isentropic fluid. Wu and Tan (1994) further generalized Moffat's theorem to rotation fluid and showed that the helicity is also conserved in three-dimensional rotation fluid in the case of the generalized force balance. Levich and Tzvethov (1984) and Lilly (1986) analyzed the relationship between the initiation and development of storm and the helicity, and showed that there are smaller diffusive and dissipative affects in the helical storm comparing with that in the non-helical storm system. Therefore, helical storm has a long life cycle. Andere and Lesieur (1977) suggested that the helicity may inhibit the downscale energy in homogeneous isotropic turbulence.

Lilly (1986) constructed the trajectories of the fluid parcels in a pure helical Beltrami flow and found that the trajectories are very similar to that of a simulation storm obtained by the three–dimensional numerical model (Klemp et al., 1981). Thus, the Beltrami flow can be regarded as the first order approximation to the storm field. The storm structure has a tendency of adjusting to the Beltrami flow. Wu et al. (1992) investigated the relationship between the nonlinear energy transition and helicity of flow in the shearing thermal convection. They proposed that the disturbances could not produce the helical structure spontaneously. The disturbances need to gain helicity from helical environmental flow, and then amplified its amplitude through the buoyancy force. Therefore, the helical mean flow plays an important role in the generation of helical structure. Moreover, the three–dimensional nonlinear energy transport among different scales is inversely correlated with the squared relative helicity of the flow. Therefore, a larger helicity always results in smaller nonlinear energy transition.

Observations and numerical simulations indicate that the long–live storms often appear in the twisted shearing environment (Davies–Jone, 1984; Weisman and Klemp, 1984). The variation of the hodograph with the height has an obvious rotational feature. The vertical velocity and vertical vorticity are maturely related (Weisman and Klemp, 1982). Droegemeier et al. (1993) investigated the influence of SREH, Bulk Richardson number (BRN) and normalized helicity density (relative helicity) NHD on the development of storm in different shearing environment flow. They argued that SREH could be thought as an indicator of the potential rotation and the identifier of the storm type. The initial environmental flow, the profile of shearing, instead of the shear itself, determinates the type of storm development. Obviously the second order inhomogeneous, i.e., the distribution of wind shear, plays an important role in the development of the storms.

Helicity has become an important physical quantity in describing the generation and development of the severe storm, and also a useful parameter for storm forecasting (Lilly, 1986; Elting, 1985; Tan and Wu, 1994). However, due to the limitation of the observation data, it is still an open question of the effect of helicity on the evolution of storms. For example, how does the helicity evolve in the developing stage of storm? Which physical mechanism controls the evolution of helicity? What is the relation between helicity and the structure of convective storms? Motivated by these questions, a typical supercell thunderstorm occurred in central Oklahom on 20 May 1977 is selected to discuss these elementary questions. The three–dimensional storm–scale numerical simulation data of the storm are used to analyze the relation between the development of storm and the helicity.

The paper is originated as follows: In Section 2 the experimental design is given. The detail analyses of simulated storm are shown in Section 3. In Section 4 the features of helicity and superhelicity of storm flow and the relationship between the helicity and the evolution of the storm are presented. Conclusions are given in Section 5.

2. Experimental design

A supercell thunderstorm event occurred near Del City, Oklahoma, on 20 May 1977. In this event, series of severe storm including sixteen tornadic storms occurred. Among them, the tornadic storm named Del City storm is observed for 2 hours during its growth stage prior to becoming tornado. This case has been well documented and studied (Ray et al., 1981; Brandes, 1981; Klemp, et al., 1981). Using Doppler–radar observation, Ray et al. (1981) investigated the three–dimensional wind structure and morphology of the storm. Brandes (1981) discussed the tornado generation and the relationship between storm inflow and tor-

nado, they concluded that rational updraft plays the major role during the tornado generation. Klemp et al. (1981) compared the three–dimensional high–resolution numerical simulation and observation of the thunderstorm and showed the detail structure of updraft, downdraft and gust front of the storm, as well as the distribution feature of vorticity. Gilmore and Wicker (1997) further investigated the influence of midtropospheric dryness on the supercell morphology and evolution with a three–dimensional and nonhydrostatic cloud model.

In this study, a nonhydrostatic, fully compressible, storm– and meso–scale prediction model named ARPS (Advanced Regional Prediction System, Xue et al., 1995), which was developed by the Center for Analysis and Prediction of Storms (CAPS), is preformed to simulate the structure and evolution of the storm. A mesh with $83 \times 83 \times 35$ is designed. The grid size is set as: $dx = dy = 1000$ m, $dz = 500$ m. Thus the physical integration area is $80 \times 80 \times 16$ km. 1.5–order TKE closure scheme and Kessler (1969) warm rain microphysics were adopted for the sub–grid and moisture process parameterization. The friction, surface physics and Coriolis force are neglected. The rigid condition is selected at the upper and bottom boundary. An elliptic thermal bubble is initialized to convection based on the homogenous environmental field of the sounding data. The center of bubble is located at 1.5 km above the surface. The magnitude of the thermal perturbation is 4K.

Figure 1 shows the initial vertical distribution of model physical quantities. The hodographs of horizontal wind u and v show a strong vertical shear (Fig. 1a, arrows indicate the moving direction of the storm). At mid– and high–level, the direction of u–component is reversed, and u comes to zero at the height of 4 km. Furthermore, the hodographs indicate a clockwise turning of the wind shear vector with the height. Figure 1b shows the profile of wet potential temperature and reveals that the air is of strong instability.

3. Evolution and structure of the storm

An evolution of the maximum updraft, maximum downdraft and model estimated radar

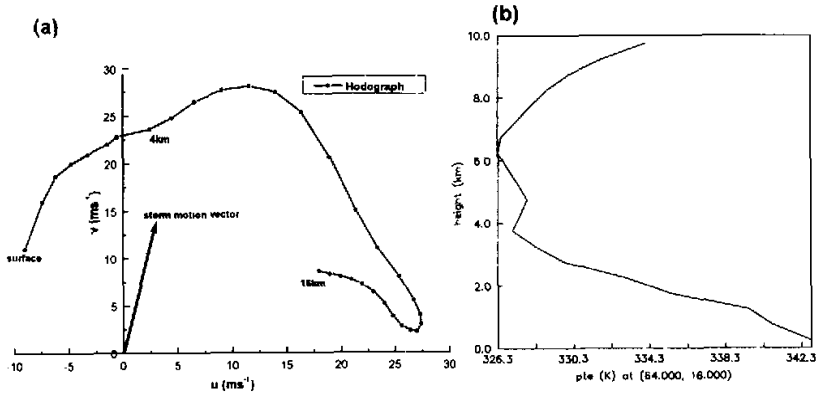

Fig. 1. Initial environmental field of the model: (a) wind hodograph (arrows indicate the moving direction of the storm); (b) vertical profile of wet potential temperature.

reflectivity (hereafter Ref) is presented in Fig. 2. From Fig. 2a it is clear that both updraft and downdraft motion increased during the period of the initial convection development, however, the updraft velocity increased more quickly. The maximum value of the model estimated radar Ref (dBZ) is increased rapidly from model time 0 to 20 min (Fig. 2b). By 20 min, the maximum Ref raised suddenly from 0 dBz to 58 dBZ, and the maximum updraft and downdraft velocity reached 19.6 ms^{-1} and -7.8 ms^{-1}, respectively. At the same time, there are two centers in the updraft area at the height of 0.25 km (Fig. 3a). In the mid–level, the updraft center has been very clear, and a downdraft flow is located at the left of the updraft flow (Fig. 3b). Therefore, we can found that the moisture is getting saturated and condensed when the disturbed air parcel moving upward, and the precipitation is induced at the low–level. The precipitation and downdraft intensified with the increasing of the updraft. The updraft center corresponded with the high value of Ref perfectly. The downdraft flow induced by the precipitation touches the surface at $t=20$ min. Therefore, the initial thermal bubble grew rapidly into a strong convection cell and began to split in the period of $t=0\sim 20$ min.

Figure 2a indicates that the intensification of the maximum updraft velocity increment is rather weak during the period of $t=20\sim 40$ min, and also the maximum downdraft increased slowly. By 40 min, two separated convective cells can be observed (Fig. 3c). The intensity of the second updraft flow developed distinctly, while the updraft of the parent cell maintains its relatively stable structure at the original position. Meanwhile, the narrow squall front of parent cell is formed near the surface, and the horizontal wind shear and convergence strengthened obviously. The intensity and extension of the downdraft that separated the updraft motion into two parts became stronger and border. As a result, the distance between the two updraft flows increased correspondingly. However, the second updraft is not so strong enough and confined only in the low level. Therefore, only one center of positive vertical velocity can be found at the mid–level. The Ref shown in Fig. 4a indicates an evident enlargement of precipitation at 40 min. This implied that the new convective cell is still in its growth stage and no precipitation formed.

In the period of $t=40$ min to 60 min, the new convection cell developed continuously and

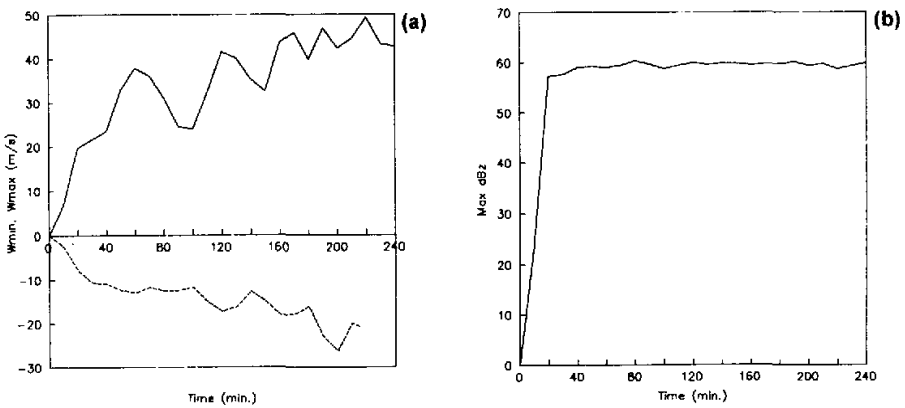

Fig. 2. Time series of (a) domain–maximum updraft (ms^{-1}, solid line) and domain–maximum downdraft (ms^{-1}, dash line); (b) domain–maximum model's estimated radar reflectivity (dBZ).

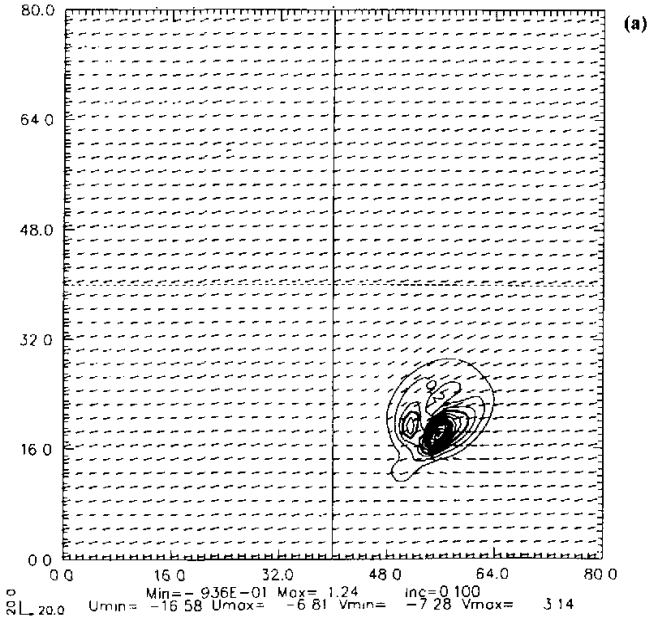
(a)
80.0
64.0
48.0
32.0
16.0
0.0
0.0
16.0
32.0
48.0
64.0
80.0
Min=-9.36E-01 Max= 1.24 Inc=0.100
Umin= -16.58 Umax= -6.81 Vmin= -7.28 Vmax= 3.14

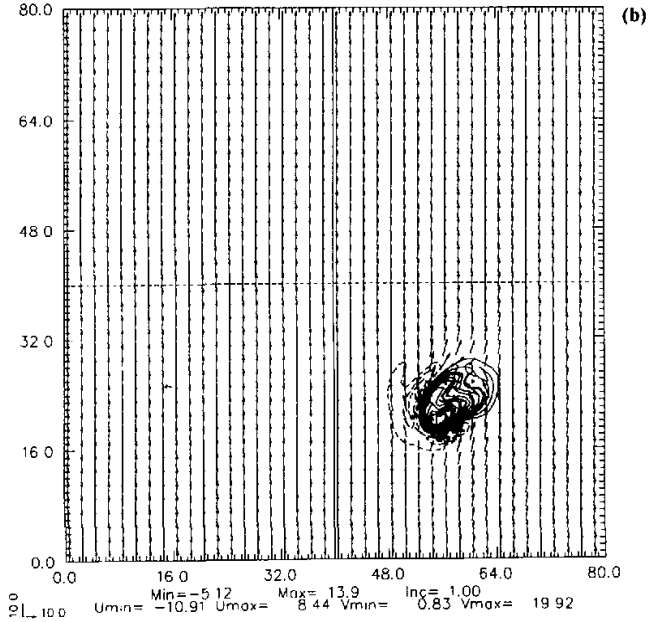
(b)
80.0
64.0
48.0
32.0
16.0
0.0
0.0
16.0
32.0
48.0
64.0
80.0
Min=-5.12 Max= 13.9 Inc= 1.00
Umin= -10.91 Umax= 8.44 Vmin= 0.83 Vmax= 19.92

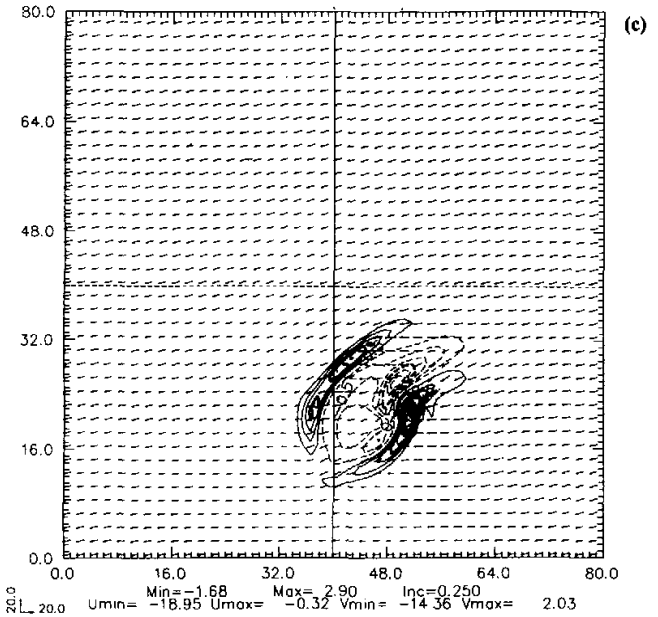
(c)
80.0
64.0
48.0
32.0
16.0
0.0
0.0
16.0
32.0
48.0
64.0
80.0
Min=-1.68 Max= 2.90 Inc=0.250
20.0
20.0 Umin= -18.95 Umax= -0.32 Vmin= -14.36 Vmax= 2.03

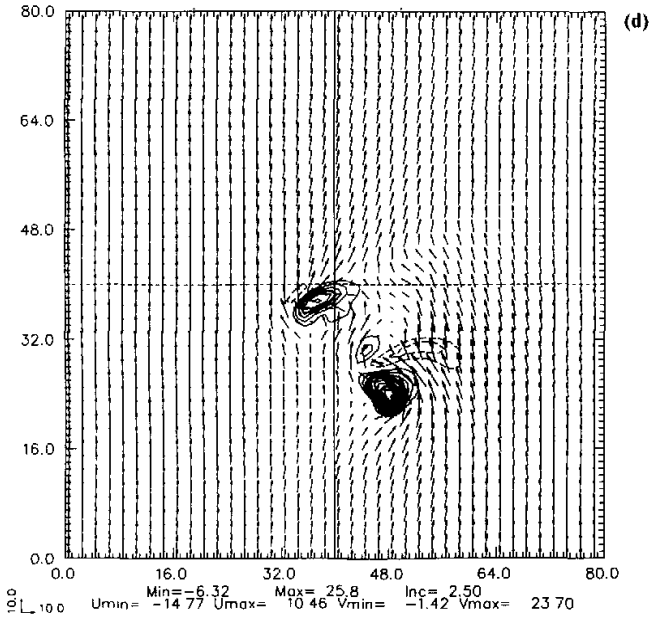
(d)
80.0
64.0
48.0
32.0
16.0
0.0
0.0
16.0
32.0
48.0
64.0
80.0
Min=-6.32 Max= 25.8 Inc= 2.50
10.0
10.0 Umin= -14.77 Umax= 10.46 Vmin= -1.42 Vmax= 23.70

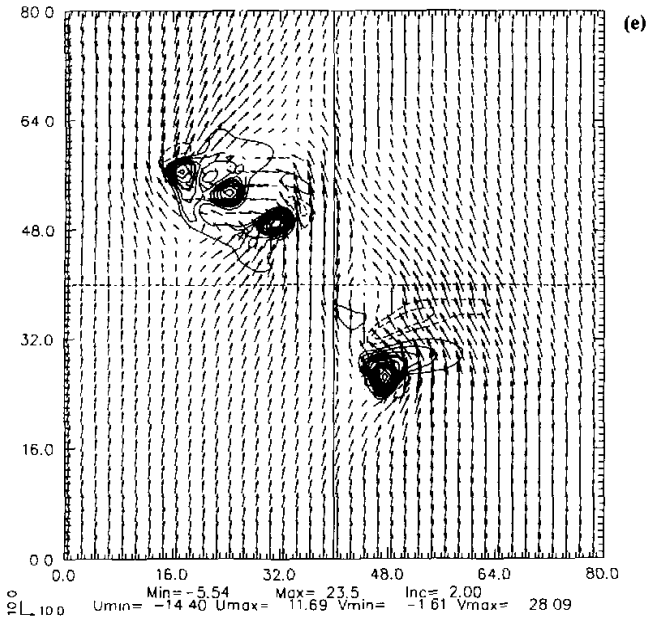

Fig. 3. System–relative wind vector and horizontal distribution of vertical velocity (ms^{-1}), the solid and dashed lines denote positive and negative values, respectively; at (a) 20 min and $z=0.25$ km, 0.1 ms^{-1}contour intervals; (b) 20 min and $z=4$ km, 1.0 ms^{-1}contour intervals; (c) 40 min and $z=0.25$ km, 0.25 ms^{-1}contour intervals; (d) 60 min and $z=4$ km, 2.5 ms^{-1}contour intervals (e) 100 min and $z=4$ km, 2.0 ms^{-1}contour intervals.

evolved into its mature phase as it moved away from the parent cell, however the parent cell still kept its steady structure and intensify at the original place. At t= 60 min, a new updraft motion emerged at the mid–level, and the downdraft appears also in the downwind side (Fig. 3d). These indicate that the updraft has developed to the mid– and high–level from the low–level, and the first splitting of storm happened. In this period, the updraft motion increased quickly again (Fig. 2a), while the downdraft performed little change. From the horizontal distribution of Ref at the surface (Fig. 4b), we can find that the new precipitation appeared in the location of the new cell. This implies that the new cell will enter its mature stage. Meanwhile, the precipitation of the parent cell presents a hook structure.

After $t=60$ min, the parent cell kept its steady structure at the original position. However, the precipitation associated with the new cell will develop continuously. The extension of the precipitation enlarged constantly and finally merged with that of the parent cell that produced a broad rainfall region. The updraft area expanded unceasingly at the mid–level and at the low level convergence strengthened. During the movement of the cell, at $t=100$ min, another new cell was generated between the two old cells, and a corresponding strong updraft emerged at the mid–level (Fig. 3e).

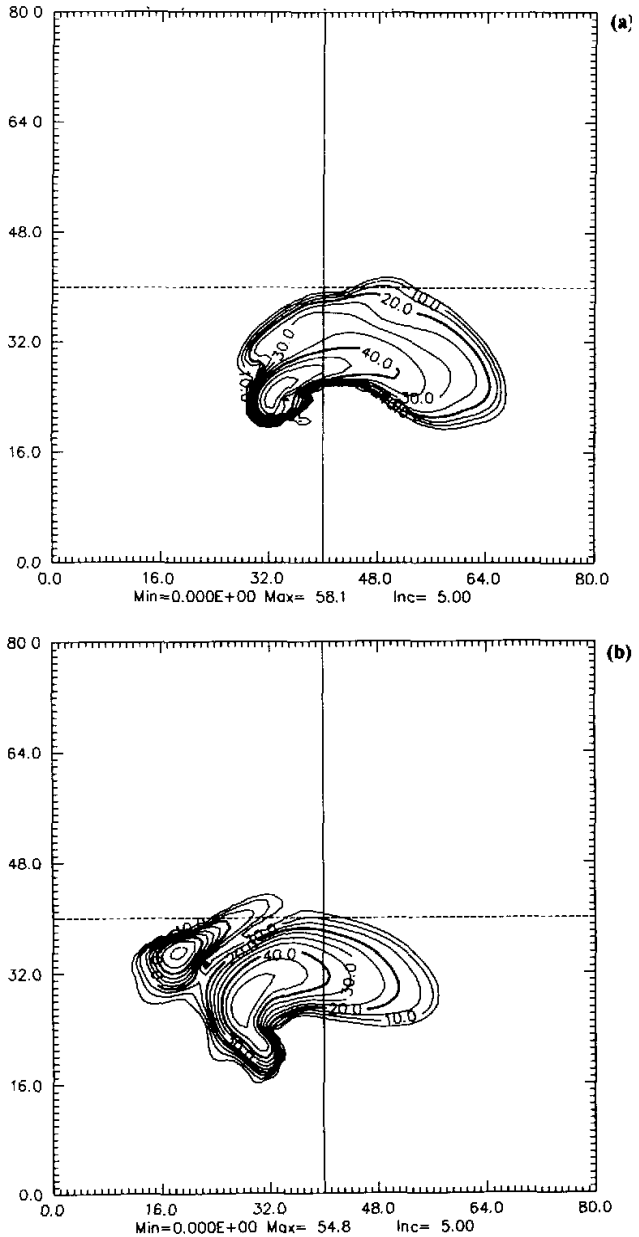

Fig. 4. Horizontal distribution of model's estimated radar reflectivity at 0.25 km MSL intervals 5.0 dBZ and at (a) 40 min; (b) 60 min.

Figures 5a and 5b show the radar observation of vertical velocity and horizontal wind at $z=1$ km and 4km at 1833 UTC, 20 May 1977, respectively (Klemp et al., 1981). The corresponding model integration time is about at $t=120$ min. The simulations of vertical velocity and horizontal wind vector at $t=120$ min and $z=0.5$ km, 4 km are shown in Figs. 5c and 5d, respectively. Comparing Fig. 5c with 5a, we can find that the simulated intensity and extension of updraft and downdraft, and horizontal wind fields are quite similar to the observations. The difference lies on some smaller scale systems, for radar observation can identify

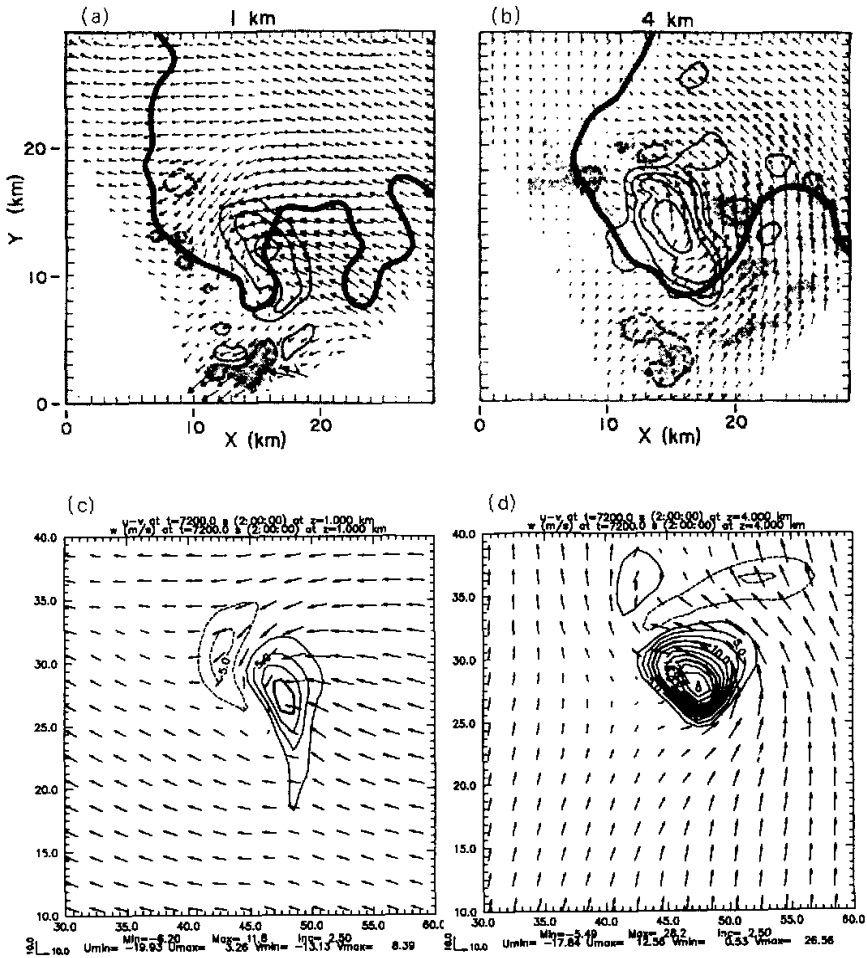

Fig. 5. Radar observation of vertical velocity and horizontal wind vectors at 1833, 20 May at elevations (a) 1 km and (b) 2 km. Updraft velocities (solid lines) and downdraft velocities (dashed lines) are contoured at 5 ms^{-1}increment. The shaded regions denote $w<-1$ ms^{-1}. They heavy solid line corresponds to 30 dBZ (from Klemp, et al., 1981). Horizontal cross sections of the modeled wind vectors and vertical velocity at 120 min at (c) 1 km and (d) 4 km. Solid lines (dashed lines) denote the updraft velocities (downdraft velocities) with the contour intervals of 2.5 ms^{-1}.

smaller scale systems, which are filtered by the numerical model. The feature is similar to the numerical simulation of Klemp et al. (1981).

Based on the above analysis, the ARPS could successfully simulate the structure and evolution of the supercell thunderstorm. With the excitation of thermal bubble, the convective storm can be initiated in the potential unstable environment atmosphere. Due to the downdraft motion, the convective cell can be split into two new separated cells. The parent cell could maintain its steady updraft structure at the original place. While the new one evolves to its mature phase, and splits again when it moves away from the parent cell.

4. Helicity and superhelicity distribution in storm

4.1 *Helicity of environmental flow*

The evolution of convection storm is closely related to the energy transport among the lager–scale environment, convection cell and small–scale turbulence. In this section, the development and maintenance of the convective storm are analyzed with the view of helicity and superhelicity. At the initial stage of the storm, the vorticity vector was oriented horizontally without the vertical component because the wind shear only appeared along the vertical. The variation of horizontal vorticity vector (ω_x, ω_y) with height is showed in Fig. 6a, where ω_x, and ω_y represents the $x-$ and $y-$ component of vorticity vector, respectively. Obviously, the variation of the horizontal vorticity vector in the vertical is inhomogeneous. With the increase of the height, the horizontal vorticity vector turned clockwise from the third quadrant at the low level to the first quadrant. Above the height of 7 km, the horizontal vorticity decreased sharply with the increase of the height. Compared with the hodograph shown in Fig. 2a, we can find that the storm inflow has a good corresponding relation with the horizontal vorticity vector. The angle between the two vector directions is small. This indicates that the rotation of the storm environment flow is mainly in the inflow direction.

The vertical distribution of helicity and its components (h_x, h_y, h_z) defined in (2) for initial environmental flow are shown in Fig. 6b. Since the initial vertical velocity is zero, h_z is also zero. Below 2 km, h_x is relatively large while h_y is relatively small. Between 2 km to 4 km, h_y has a main contribution to the helicity. Above the height of 7 km, h_y is decreased and h_x become the main contributor to helicity of flow again. At the lower and upper level, the u–component of the inflow is prevailing, however, the v–component is dominant at the mid–level. These features indicate that the initial enviromental field has a helical structure. The helicity is large at the low and high level, and is small at the mid–level. This feature stimulates the nonlinear energy transport activity and is favorable to the development of convection at the mid–level that agrees with the simulation shown in Section 3.

4.2 *Horizontal structure of helicity*

By 20 min into the simulation, the parent convection cell has entered its mature stage and began to split. The horizontal distribution of helicity at 20 min and $z=0.25$ km is shown in Fig. 7a. The helicity increased evidently in the upwind side of the convection, however, decreased in the downwind side of the convection cell where the splitting of convection is occurring. The decreasing of helicity could intensify the nonlinear energy cascade and leads to the development of disturbance with the increasing of time. With the surface gust front of parent cell appearing, the higher helicity near the gust front is increased (Fig. 7b). At this time, the splitting process of parent convection cell has finished and the new cell will develop. With the development and movement of the new cell, the low–value helicity will move away as well and

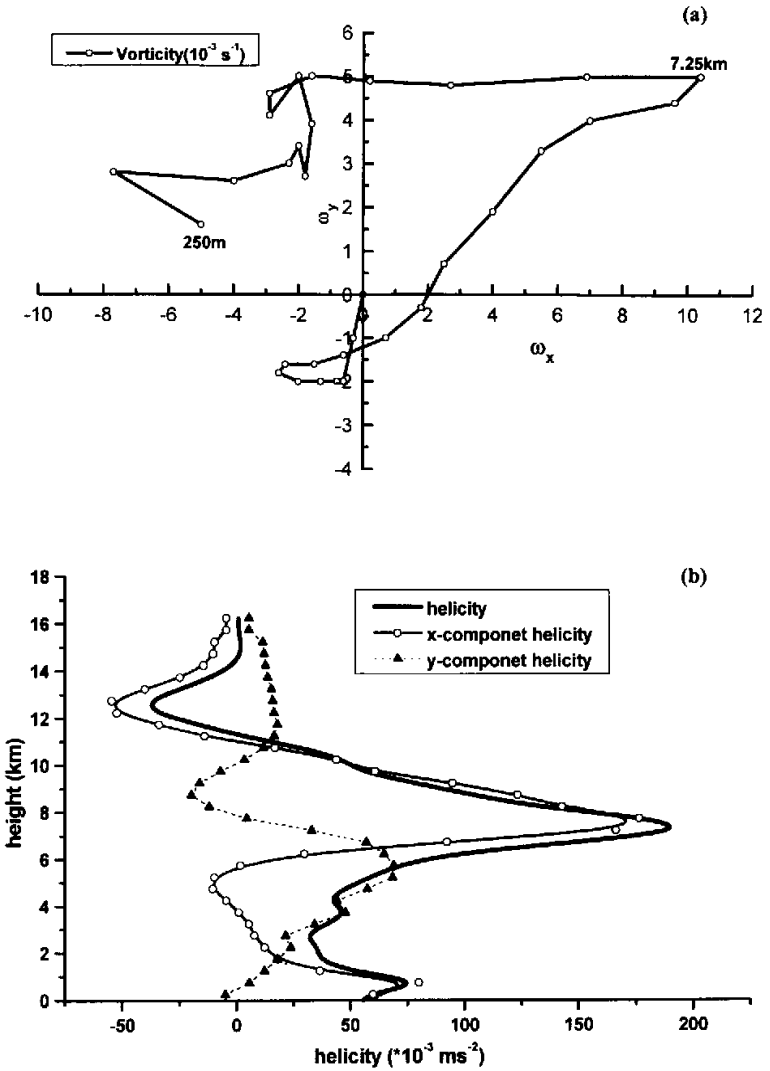

Fig. 6. Initial vorticity and helicity of the environmental field; (a) the hodograph for the horizontal vorticity vector, the marks on profile denote the sea level elevation; (b) the vertical profile of helicity and its components in x– and y–direction.

decrease further.

At $t=60$ min, the precipitation and separated up–down structure of vertical motion associated with the new convection cell appear. The feature means that the new cell will approach its mature stage. At the low and mid–level, a high helicity merges in the place between the two convective cells (Fig. 7c). This implies that the helical structure of the cell has formed. While the existence and maintenance of the negative helicity area implied that the new cell

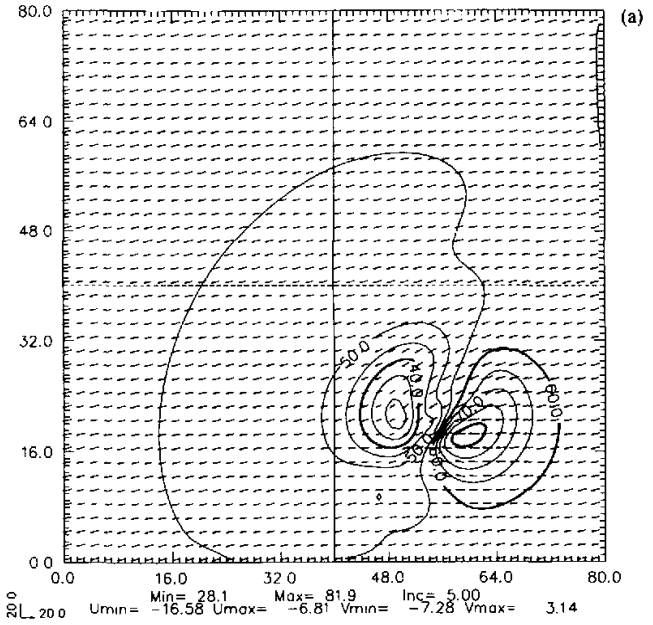
(a)
80.0
64.0
48.0
32.0
16.0
0.0
0.0
16.0
32.0
48.0
64.0
80.0
Min= 28.1 Max= 81.9 Inc= 5.00
Umin= -16.58 Umax= -6.81 Vmin= -7.28 Vmax= 3.14

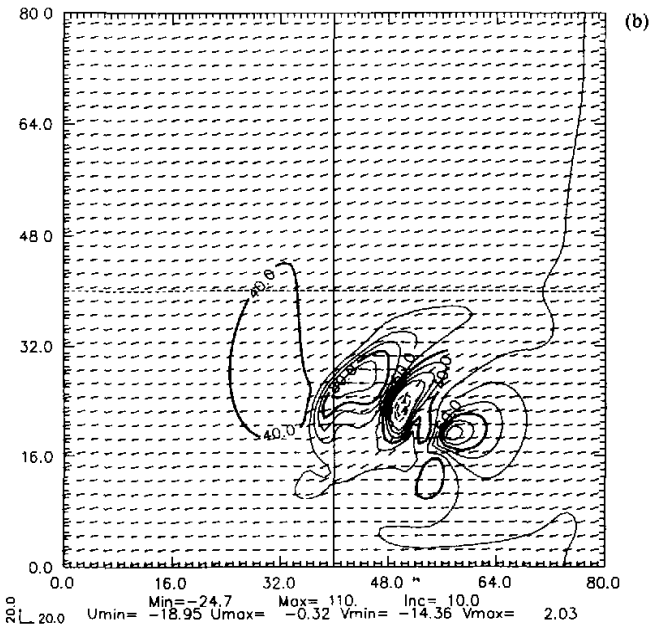
(b)
80.0
64.0
48.0
32.0
16.0
0.0
0.0
16.0
32.0
48.0
64.0
80.0
Min=-24.7 Max= 110. Inc= 10.0
Umin= -18.95 Umax= -0.32 Vmin= -14.36 Vmax= 2.03

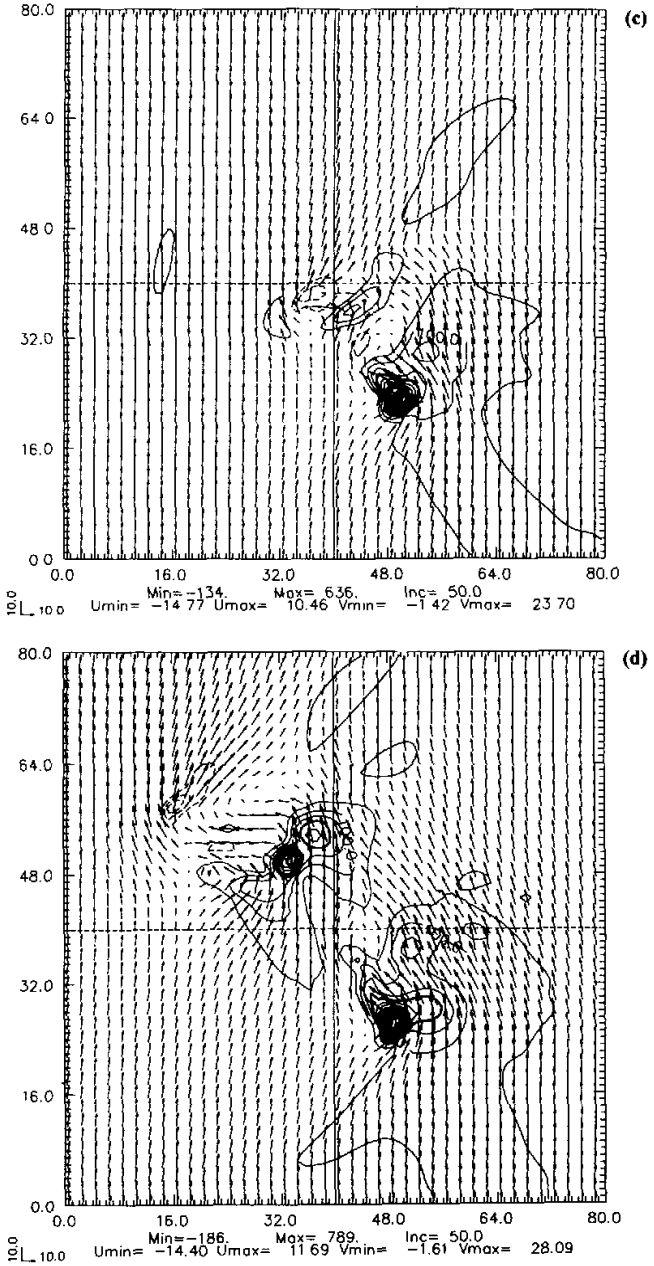

Fig. 7. Horizontal distribution of helicity (10^{-1}ms^{-2}) at (a) 20 min and 0.25 km, contour interval 5.0 (b) 40 min and 0.25 km, contour interval 10.0; (c) 60 min and 4.0 km, contour interval 50.0; (d) 100 min and 0.25 km, contour interval 50.0.

would continue to develop and split again. Figure 7d shows the horizontal distribution of helicity at 100 min and $z=0.25$ km. Clearly, the both two old cells corresponded to the large positive helicity that inhibited the nonlinear energy cascade and leads to maintain the long life of the convection, however, the negative helicity only appeared near the new cell.

Figures 8a and 8b show the horizontal distribution of the low-level vertical velocity and helicity at 240 min, respectively. In Fig. 8a, there are two mature storm cells. One located on the right hand was split from the initial parent cell, the other on the upper left hand was split from the right-hand cell. At this moment, both the convective cells are mature and have a similar horizontal structure of vertical velocity. The helicity of both cells displays the similar horizontal structures also. Therefore, the helicity will be adjusted to the similar structure when the convection cell develops toward its mature structure. This feature is similar to the suggestion by Lilly (1986) that the mature rotational convective storm have a tendency of adjustment to the Beltrami flow.

4.3 *Variation of the helicity*

An evolution of the maximum and minimum helicity at $z=0.25$, 4.0 and 7.0 km is shown in Fig. 9. In order to analyze the variation of helicity, the helicity shown in Fig. 9 has been deducted the initial helicity at the corresponding height. From Fig. 9 it is evident that helicity at different height is increased distinctly in the first 20 minutes, which is similar to the feature shown in Fig. 2a. At the same time, the minimum helicity evolved toward the negative value.

In the development stage of storm, the smaller helicity is beneficial to the development of the nonlinear and leads the convective storm system to absorb the available potential energy from large-scale environmental flow. As the convection system evolved toward its mature phase, the storm adjusted to the helical structure and the helicity increased. Meanwhile, the helicity density adjusted toward the maximum value of helicity. The increase of helicity, on one hand, inhibited the storm to absorb energy from large scale, and on the other hand, depressed the dissipation process of the convection cell, which is good to maintain the long life cycle of the storm.

4.4 *Horizontal distribution of the superhelicity*

The variation of helicity controls the energy transport among the different scale and affects the evolution and life cycle of the convective storm. Hide (1989) introduced the superhelicity density concept to investigate the friction effect on the variation of helicity. Superhelicity is defined as

$$h_\omega = \vec{\omega} \cdot \nabla \wedge \vec{\omega}. \tag{7}$$

It reflects the twisting structure of the vorticity field. In the Beltrima flow, the superhelicity is a synthesized quantity of helicity, enstrophy and kinetic energy. Kide et al. (1991) showed that the superhelicity dominates the temporal variation of helicity correspondingly by the effect of viscosity.

$$\frac{d}{dt}\int_\tau h_v \, d\tau = -2\nu \int_\tau h_\omega \, d\tau, \tag{8}$$

where ν is the viscosity coefficient of the fluid.

The horizontal distributions of low-level superhelicity as defined in (7) at 40 min and 100 min are shown in Figs. 10a and 10b, respectively. Comparison of Fig. 10a with Fig. 4c shows

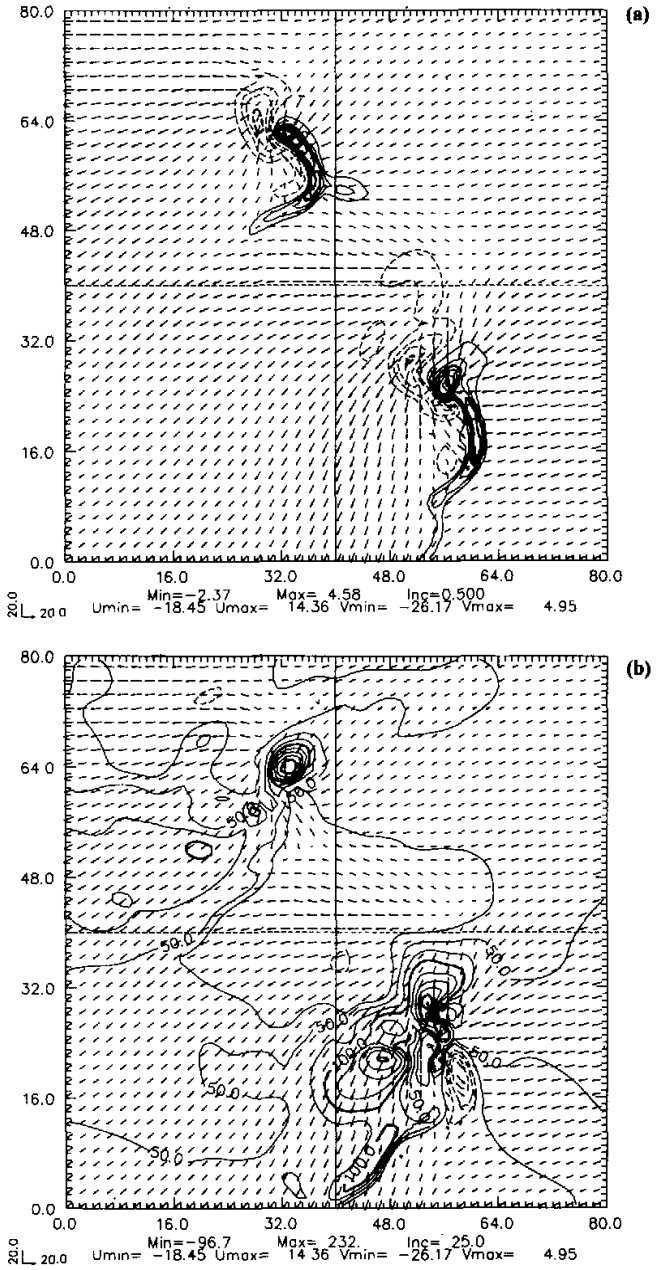

Fig. 8. Horizontal distribution at 240 min and 0.25 km MSL for (a) vertical velocity, contour inteval 0.5 ms^{-1}; (b) helicity, contour interval $2.9 \times 10^{-1} ms^{-2}$.

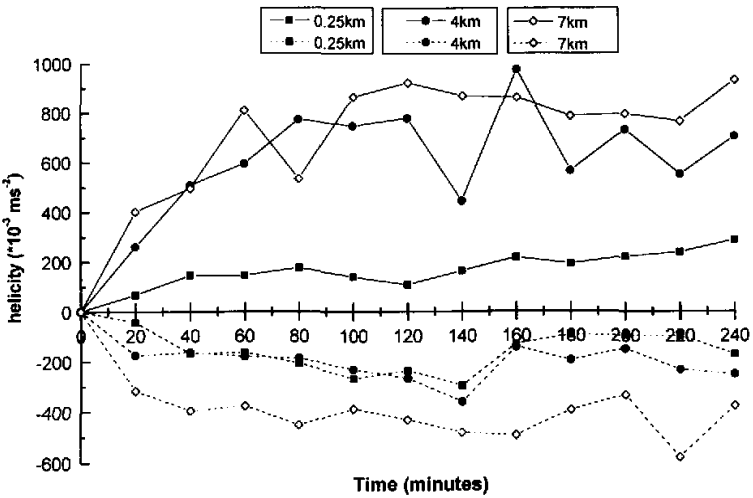

Fig. 9. Time series of the model domain–maximum and minimum helicity ($10^{-3}ms^{-2}$).

that both the centers of parent convection and surface squall front correspond to the positive superhelicity, however, the negative superhelicity corresponds to the new cell that splits from the parent cell. After the new convection cell enters its mature stage, the negative superhelicity becomes positive correspondingly (Fig. 10b).

During the development processes of the convection, not only the velocity vector and vorticity vector adjust to parallel each other to form the helical structure that is similar to the Beltrima flow, but also the higher order vorticity field adjusts too. The superhelicity adjusts from the negative value toward positive one. According to (8), the negative superhelicity is favorable to the increase of the volume integration of helicity density at the developing stage of storm if the viscosity is taken into account. This is identical to the variation tendency of the helicity. The superhelicity could suppress the increasing of helicity as soon as it becomes positive. Meanwhile the convection cell has entered its mature stage. In short, superhelicity can help one to understand the adjustment of helicity in the developing process of convective storm and can be used as a qualitative indictor to mark the developing stage of convective storm.

5. Conclusion

In this paper, a nonhydrostatic and three–dimensional storm–scale model ARPS was used to simulate the development of a supercell thunderstorm. The effect of helicity and superhelicity on the development and maintenance of convective storm was analyzed and discussed. The initial environment fields of the storm have an obvious helical structure. The rotation mainly appears in the direction of the inflow of storm. Such structure of environmental flow is benefited to twisting of the horizontal vortex tube and producing vertical component of vorticity that induces a rotational convective storm.

In the developing stage, low helicity is favorable to the energy cascade from large scale to

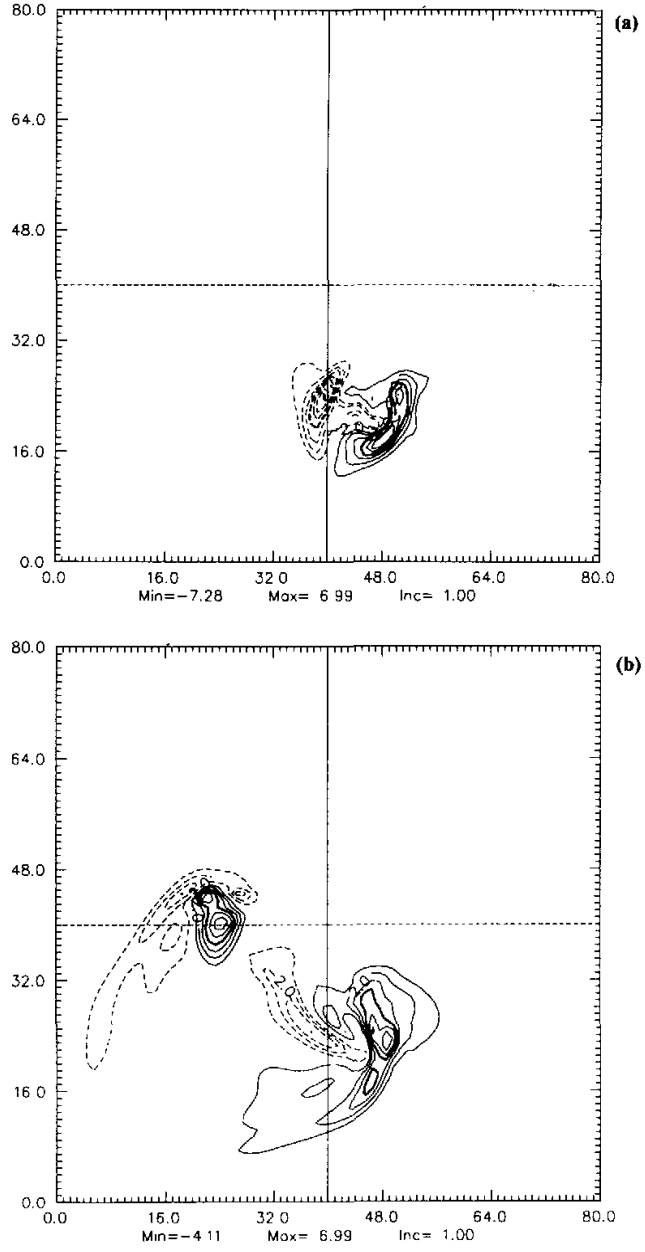

Fig. 10. Horizontal distribution of superhelicity at 0.25 km MSL. Solid and dashed lines denote positive and negative values, respectively; (a) 40 min, contour interval is $1.0 \times 10^{-7} m^{-1} s^{-2}$; (b) 100 min, contour interval $1.0 \times 10^{-7} m^{-1} s^{-2}$.

convection scale and accelerates the development and splitting of convection. However, when the storm evolves towards its mature phase, high helicity effectively inhibits the dissipation of energy that is a help to the maintenance of convection system. The convective storm has a tendency of adjusting to the Betrami flow and towards a high helicity structure.

If viscosity is considered, the superhelicity reflects the temporal variation of the helicity. Negative helicity leads to the increase of helicity. In general, superhelicity is negative in the developing phase and turns to positive when convection approaches the mature period. Therefore, superhelicity can be used to identify whether the storm is mature or not. In this paper only the evolution of helicity is discussed. Many issues need to be further discussed. For example, what is the relationship among helicity and other dynamical quantities like circulation and potential vorticity? What is their relative importance in the development and maintenance of storm system?

We thank to Mr. Zhang Jin who provided much helpful support in this research work. The simulations were made using the Advanced Regional Prediction System (ARPS) developed by the Center for Analysis and Prediction of Storms (CAPS), University of Oklahoma. CAPS is supported by National Science Foundation and the Federal Aviation Administration through combined grant ATM92-20009.

REFERENCES

Andre, J. C., and M. Lesieur, 1977: Influence of helicity on the evolution of isotropic turbulent at high Reynolds number. *J. Fluid Mech.*, **82**, 187–207.

Brandes, E. A., 1981: Finestructure of the Del City–Emond Tornadic Mesocirculation. *Mon. Wea. Rev.*, **109**, 635–647.

Davies–Jones, R. P., 1984: Streamwise vorticity: the origin of updraft rotation in supercell storms. *J. Atmos. Sci.*, **41**, 2991–3006.

Davies–Jones, R. , D. Burgess, and M. Foster, 1990: Test of helicity as a tornado forecast parameter. Preprints, 16th Conf. Severe Local Stroms, Kananaskis Park; AB. Camda, *Amer. Meteor. Soc.*, 588–592.

Droegemeier, K. K, S.M. Lazarus, and R. Davies–Jones, 1993: The Influence of helicity on numerically simulated convective storms. *Mon. Wea. Rev.*, **121**, 2005–2029.

Elting, D. 1985: Some aspects of helicity in atmospheric Flows. *Beitr. Phys. Atmos.*, **58**, 88–100.

Gilmore, M. S., and L. J. Wicker, 1997: The Influence of Midtroposheric Dryness on Supercell Morphology and Evolution. *Mon. Wea. Rev.*, **126**, 943–958.

Hide, R., 1989: Superhelicity, helicity and potential vorticity. *Geophys. Astrophys. Fluid Dynamics*, **48**, 69–79.

Kida, S., M. Takaoka, and F. Hussain, 1991: Collision of two vortex rings. *J. Fluid Mech.*, **230**, 583–646.

Kessler, E., 1969: On the distribution and continuity of water substance in atmospheric circulation. *Meteor. Mongor.*, **10, No. 32**, *Amer. Metor. Soc.*, 84–87.

Klemp, J. B., R. B. Wilhelmson, and P. J. Ray, 1981: Observed and numerically structure of a mature supercell thunderstorm. *J. Atmos. Sci.*, **38**, 1558–1580.

Levich, E., and E. Tzvetkov, 1984: Helical cyclogenesis. *Phys. Lett.*, **100A**, 53–56.

Lilly, D. K., 1986: The structure, energetics and propagation of rotating convective storms. Part I: Helicity and storm stabilization. *J. Atmos. Sci.*, **43**, 126–140.

Moffat, H. K., 1969: On the knottedness of tangled vortex lines. *J. Fluid Mech.*, **35**, 117–128.

Ray, P. S., B. C. Johnson, K. W. Johnson, J. S. Braderry, J. J. Stephens, K. K. Wagner, R. B. Wilhelmson, and J. B. Klemp, 1981: The morphology of several tornadic storms on 20 May. *J. Atmos. Sci.*, **38**, 1643–1663.

Tan Zhemin and Wu Rongsheng, 1994: Helicity dynamics of atmospheric flow. *Adv. Atmos. Sci.*, **11**, 175–188.

Weisman, M. L., and J.B. Klemp, 1982: The dependence of numerically simulated convective storms on vertical wind shear and buoyancy. *Mon. Wea. Rev.*, **110**, 504–520.

Weisman, M. L., and J. B. Klemp, 1984: The structure and classification of numerically simulated convective storms

in directionally varying wind shears. *Mon. Wea. Rev.*, **112**, 2479–2498.

Wu Rongsheng and Tan Zhemin, 1989: Conservative laws on generalized vorticity and potential vorticity and its applications. *Acta. Meteorologica Sinica*, **47**, 436–442.

Wu, W. S., D. K. Lilly, and R. M. Kerr, 1992: Helicity and thermal convection with shear. *J. Atmos. Sci.*, **49**, 1800–1809.

Xue, M., K. K. Droegemeier, V. Wong, A. Shapiro, and K. Brewster, 1995: *Advanced Regional Prediction System* (*ARPS*) Version 4.0 User's Guide. Center for Analysis and Prediction of Storms (CAPS), University of Oklahoma, 320pp.

对流性强风暴系统的螺旋度动力学研究

费世强　　谈哲敏

摘　要

利用风暴尺度的数值模式 ARPS 成功地模拟了 1977 年 5 月 20 日在美国 Oklahoma 州 Del City 的一次强对流风暴过程. 其模拟结果与实际的观测非常接近, 模式积分 40 分钟, 初始对流单体发生了分裂, 产生了新的对流单体。原有对流单体在原地维持成熟的结构, 表现出较强的稳定性, 而分裂出的新单体在移动过程中,逐渐向成熟位相发展, 并且又分裂出新的单体. 利用模拟结果, 着重讨论了风暴发展过程中螺旋度和超螺旋度的空间结构和时间演变特征, 以及在强风暴系统的对流发展过程中的动力学作用. 初始环境场的螺旋性结构有利于风暴的发展. 在风暴发展阶段, 低螺旋度有利于大尺度向对流尺度的能量串级, 而在风暴成熟阶段,高螺旋度则有利于对流单体的能量维持, 从而形成长生命周期的对流系统. 在风暴的发展过程中, 风暴流场结构具有向 Beltrami 流结构的调整趋势, 螺旋度向高值发展. 超螺旋度在流体粘性作用的影响下, 可反映出螺旋度密度空间积分的时间变化趋势, 负的超螺旋度可使螺旋度增加。在对流风暴发展阶段, 超螺旋度为负值,对流单体的结构螺旋性增强、螺旋度的增大, 在风暴到达成熟阶段后, 超螺旋度转为正值。因此, 超螺旋度可用来标志对流风暴系统的成熟程度.

关键词: 对流风暴, 螺旋度, 超螺旋度